Int. J. Heat Mass Transfer. Vol. 10, pp. 1661–1676. Pergamon Press Ltd. 1967. Printed in Great Britain

A THEORETICAL AND EXPERIMENTAL INVESTIGATION OF DIFFUSION-CONTROLLED ELECTROLYTIC MASS TRANSFER BETWEEN A FALLING LIQUID FILM AND A WALL

A. IRIBARNE, A. D. GOSMAN and D. B. SPALDING

Imperial College of Science and Technology, Department of Mechanical Engineering, Exhibition Road, London, S.W.7

(*Received* 17 *February* 1967 *and in revised form* 24 *May* 1967)

Abstract—Measurements have been obtained of the mass-transfer coefficient between a falling liquid film and a vertical surface; the diffusion-controlled electrolytic mass-transfer technique was employed. The measurements are compared with predictions based on an adaptation to film flows of a theory given by one of the present authors for heat or mass transfer through boundary layers. There is good agreement between theory and experiment provided that the film Reynolds number is outside the range of approximately 700–1000.

NOMENCLATURE

A_*, constant in Van Driest total-viscosity expression;
A, area of mass-transfer surface;
$a_{g,x}$, component of gravitational acceleration acting in the direction of the flow;
$\mathscr{D}_t$, eddy diffusivity;
$\mathscr{D}$, molecular diffusivity;
F, Faraday's constant (= 96 500 A-s/g-equivalent);
g, local mass-transfer coefficient;
$\bar{g}$, average mass-transfer coefficient;
I, diffusion-controlled current;
L, length of mass-transfer surface;
L^+, non-dimensional length;
$\dot{m}''$, local mass flux of diffusing species;
$\overline{\dot{m}''}$, average mass flux of diffusing species;
M_{Fe}, molecular weight of ferricyanide ion (= 329·3);
n, valence change in electrochemical reaction;
$\bar{N}_g$, $\equiv \bar{g}N_{Sc}/(\mu\rho^2 a_{g,x})^{\frac{1}{3}}$, a non-dimensional mass-transfer coefficient;
N_{Re}, Γ/μ, film Reynolds number;
N_{Sc}, laminar Schmidt number;
$N_{Sc,t}$, turbulent Schmidt number (= 0·9);
S, non-dimensional local conductance;
$\bar{S}$, non-dimensional average conductance;
$\bar{u}$, time-mean velocity along the wall;
u^+, non-dimensional time-mean velocity along the wall;
x, distance along wall;
x^+, non-dimensional distance along wall;
y, distance from and normal to wall;
y^+, non-dimensional distance normal to wall.

Greek symbols

Γ, mass flow rate of liquid per unit width of film;
δ, mean film thickness;
δ^+, non-dimensional mean film thickness;
ε_u^+, non-dimensional total viscosity;
ε_φ^+, non-dimensional total diffusivity;
θ, angle of surface with the horizontal;
$\varkappa$, constant in Van Driest total-viscosity expression;
μ, molecular viscosity;
μ_t, eddy viscosity;
ρ, density of the liquid;
σ, surface tension coefficient;

τ, shear-stress in the film in a plane parallel to the surface;
φ, concentration of diffusing species (g/g solution).

Subscripts
G, main stream;
S, wall.

1. INTRODUCTION

1.1. *The problem*

FIGURE 1 illustrates a solid surface, inclined at angle θ with the horizontal, down which flows a film of liquid. Mass transfer of a chemical species i takes place between the solid and the film in the region $0 < x < L$, where x is the distance along the surface in the direction of flow; in this region the concentration of i at the interface is caused to equal zero.

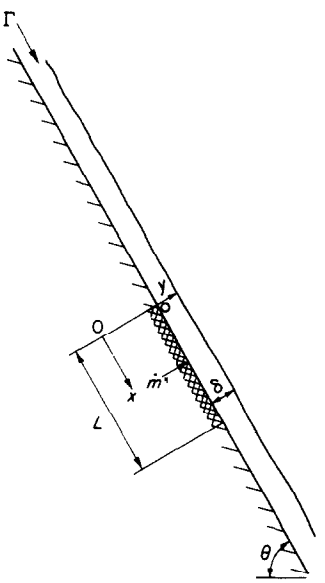

FIG. 1. Mass transfer between a falling liquid film and an inclined surface; the active portion of the surface is represented by cross-hatching.

We seek to calculate the mass flux $\dot{m}''$ as a function of: the mass flow rate of the film per unit width Γ, the concentration of i in the bulk of the fluid φ_G, the position on the surface x, the angle of inclination θ, and the transport properties of the fluid.

1.2. *Motivation for the research*

(1) *Practical importance.* Film flows are encountered in many common types of industrial equipment, including: coolers, gas–liquid contactors, condensers, evaporators and rectifiers. Some recent applications are: (a) the cooling of the walls of rocket nozzles and spacecraft by the interposition of a liquid film between the surface to be protected and the hot gases; and (b) the transfer of heat from the core of a nuclear reactor by two-phase heat transfer. In such applications, the liquid often flows in the form of a film on the walls of the cooling channels.

(2) *Theoretical significance.* In the present work, a theoretical and experimental investigation of the problem has permitted testing of the validity of the assumption that the distributions of the total viscosity and the velocity in the film can be described by relations developed for flows in pipes and boundary layers.

1.3. *Outline of the present paper*

The work reported here has two components:

(1) Measurements are presented of the mass-transfer coefficient between a falling liquid film and a vertical surface; the diffusion-controlled electrolytic mass-transfer technique has been employed. The measurements, which are described in Section 2.1, embrace a range of flow rates and fluid properties which are listed in Table 1.

The results, plotted in the form of a dimensionless mass-transfer coefficient vs. the film Reynolds number, are shown in Figs. 3(a–d).

(2) A straightforward adaptation to film flows is presented of one of the recent theories [1] for heat or mass transfer through uniform-property boundary layers. The details of the adaptation are given in Appendix A, and the main results are outlined in Section 2.3. It is shown [see Figs. 5(a–d)] that the experimental data for Reynolds numbers less than approxi-

Table 1. Range of independent variables covered in the mass-transfer experiments and fluid property data for the solutions employed

Solution No.	N_{Sc}	Range of N_{Re}	Range of L^+	NaOH Conc. (g-mol/l)	ρ (g/cm^3)	μ (g/s cm)	σ (dyn/cm)	Data appear in figures
1.	1400 ± 7%	110–4900	170–2400	0·521	1·02	0·01032	72·25	3(a) and 5(a)
2.	2550 ± 7%	50–3600	125–5000	2·08	1·08	0·01445	76·75	3(b) and 5(b)
3.	6250 ± 5%	10–2200	80–6500	4·086	1·154	0·02353	81·75	3(c) and 5(c)
4.	18400 ± 5%	3–1200	50–4500	6·103	1·221	0·04129	86·8	3(d) and 5(d)

Note: Fluid-property data were taken from Bazan and Arvia [19] and Duffield [20].

mately 700 agree well with the version of the theory which is valid for conditions when the concentration boundary layer is confined to a region of laminar flow. Above a Reynolds number of approximately 1000, the data agree with the version which holds for turbulent flows. Intermediate Reynolds numbers yield data which lie between the predictions of the two versions of the theory.

2. DETAILS OF THE INVESTIGATION

2.1. *The mass-transfer experiments*

In the present investigation, a continuous flow of liquid was introduced on the outer surface of a vertical cylinder. Measurements were made of the average rate of mass transfer of the chemical species $Fe(CN)_6^{3-}$ (ferricyanide ion) from the bulk liquid to the surface of short electrically isolated sections of the cylinder. The ferricyanide ion took part in the following electrochemical reaction at the surface:

$$\underset{\text{ferricyanide ion}}{Fe(CN)_6^{3-}} + \underset{\text{electron}}{e^-} \rightarrow \underset{\text{ferrocyanide ion}}{Fe(CN)_6^{4-}}. \qquad (2.1.1)$$

The mass-transfer surface, which we term the cathode, was electrically connected to another section of the cylinder of much larger surface area, termed the anode, at which occurred the reverse reaction to (2.1.1). The anode and the cathode formed the two electrodes of an electrochemical cell. The cathode reaction (2.1.1) was initiated and maintained by the application of an electric potential between the electrodes. The rate of reaction, which can be determined from the current which flows between the electrodes, increases approximately exponentially with increasing applied potential, until the overall rate is limited by the rate of diffusion (molecular and convective) of the ferricyanide ion from the bulk solution to the cathode surface. Under these conditions, (a) the current becomes independent of the applied potential, and (b) the concentration of ferricyanide ion at the surface falls to a value which is negligible in comparison with the bulk value. The mass-transfer process is then said to be diffusion-controlled. Further details of the electrochemical technique can be found in [2] and [3], among others.

The boundary condition for the associated mass-transfer problem is one of a step change in the concentration at the wall: upstream of the plane $x = 0$ (the upstream edge of the cathode), the concentration is everywhere uniform; in the region $0 < x < L$, where L is the length of the cathode, the concentration at the wall is held at a new value which is effectively zero.

In the present work we are interested in the average mass-transfer coefficient $\bar{g}$, which is defined and related to the measured variables as follows:

$$\bar{g} \equiv \frac{\bar{m}''}{\varphi_G - \varphi_S} = \frac{M_{Fe} I}{nF\varphi_G A} \qquad (2.1.2)$$

where

$A \equiv$ area of the mass-transfer surface,
$F \equiv$ Faraday's constant (= 96500 A-s/g equivalent),
$\bar{g} \equiv$ average mass-transfer coefficient,
$I \equiv$ diffusion-controlled current,
$M_{Fe} \equiv$ molecular weight of ferricyanide ion (= 329·3 g/g-mole),
$\bar{m}'' \equiv$ average mass flux of ferricyanide ion,
$\varphi_G, \varphi_S \equiv$ concentration of ferricyanide ion in the bulk solution and at the surface, respectively, (g ferricyanide ion/g solution),
$n \equiv$ valence change in the reaction (= 1).

Apparatus. The test section employed in the experiments is shown schematically in Fig. 2; it was in the form of a vertical cylinder approximately 150 cm in length and 3·3 cm in diameter. From top to bottom, the section was made up of: (1) a porous stainless steel flow distributor, 10 cm in length; (2) a 38·5-cm length of perspex which served as a hydrodynamic entry length; (3) the mass-transfer section, of total length 99·6 cm, which was composed of fifteen electrodes. Each electrode consisted of a length of nickel tube, electrically insulated from its neighbors by a 0·005-cm thickness of fluon. The table which accompanies Fig. 2 lists the length of the individual electrodes, which are designated in Fig. 2 by a number. Electrodes 4–14, which ranged in length from 0·3 to 2 cm, were the principal electrodes used in the experiments; number 15 served as a large anode. Cathode 2 and the associated anode 3 were used for control measurements, which, when compared with the readings taken with 14, provided an indication as to whether the flow was hydrodynamically fully developed over the principal electrodes. Over the full range of variables covered in the present experiments, no differences were detectable between the readings from 2 and 14; hence we infer that the calming section ensured fully developed flow.

The electric circuit employed for the mass-transfer measurements was designed so that

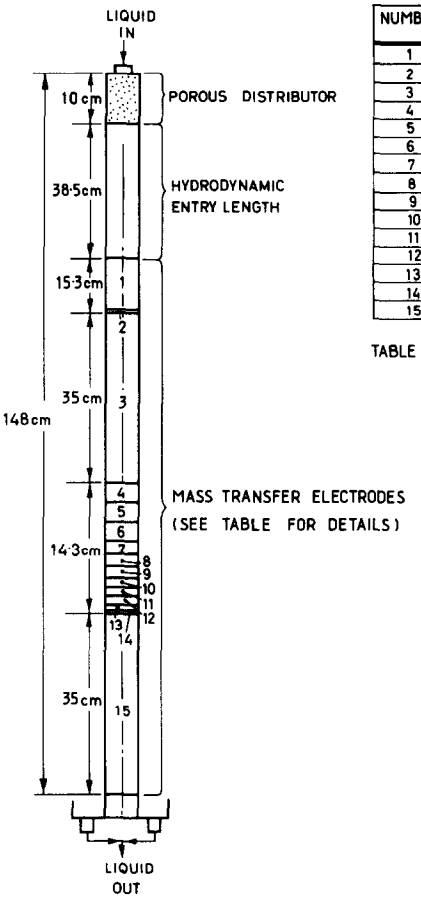

NUMBER	LENGTH cm
1	15·0
2	0·3
3	35·0
4	2·0
5	2·0
6	2·0
7	1·5
8	1·5
9	1·5
10	1·0
11	1·0
12	1·0
13	0·5
14	0·3
15	35·0

TABLE OF ELECTRODE LENGTHS

FIG. 2. Schematic diagram of the mass-transfer test section.

it was possible to select any combination of electrodes, to apply a known potential difference between them, and to measure the time-average mass-transfer current. The remainder of the apparatus was conventional in design and served to provide a metered, controlled-temperature (25 ± 0·5°C) flow of liquid to the test section.

Procedure. The procedure employed in the tests was as follows: the liquid flow-rate was set, and the electrical connections were arranged for the selected anode–cathode system. In all the tests, the electrodes downstream of the measuring cathode were employed as additional anodes, in order to minimize the potential

drop in the liquid film. Measurements were then made of the current as a function of the applied potential; hence the diffusion-controlled current was determined. The measurements were then repeated for successively longer cathodes (in some instances several electrodes were coupled together) until it was no longer possible to obtain a diffusion-controlled current. The upper limit on the electrode length was imposed by the ohmic drop in the electric potential which occurred in the film. Measurements of the ferricyanide ion concentration were made at regular intervals during the tests.

Details of liquids. The liquids employed in the experiments were made up of equimolar (0·005 g-mol/l) concentrations of potassium ferricyanide and potassium ferrocyanide in solutions of sodium hydroxide and distilled water. The transport properties of the solutions, in particular the viscosity and the diffusion coefficient of the ferricyanide ion, were varied by varying the concentration of sodium hydroxide in the range 0·5–6 g-mol/l; the corresponding range of N_{Sc} ($\equiv \mu/\rho\mathscr{D}$, where μ is the viscosity of the solution, ρ is the density, and $\mathscr{D}$ is the diffusion coefficient of the ferricyanide ion) was approximately 1400–18000. The fluid properties of the solutions are listed in Table 1. The table also lists the values of nondimensional quantities which will be defined later.

Measurement of fluctuations in the mass-transfer rate. Waves could be seen on the surface of the film over virtually the complete range of flow rates for each of the liquids employed. A limited number of instantaneous mass-transfer rates were measured in order to ascertain if the waves caused large-scale oscillations. Solution No. 2 was used; cathode No. 14 was employed as the measuring electrode. It was found that over the greater part of the range of N_{Re} from 50 to 3600, the oscillations in mass-transfer rate were small—of the order of ± 2 per cent of the time-averaged rate. Maximum values of the order of ± 8 per cent were observed at large N_{Re}, and appeared to coincide with the passage over the electrode of large-amplitude waves of the type termed "roll waves" in the film-flow literature [21].

2.2. *Results*

The mass-transfer data obtained for the four solutions employed in the tests are shown in Figs. 3(a–d). The ordinate in the figures is a non-dimensional mass-transfer coefficient $\bar{N}_g[\equiv \bar{g}N_{Sc}/(\mu\rho^2 a_{g,x})^{\frac{1}{3}}]$ and the abscissa is the film Reynolds number $N_{Re}(\equiv \Gamma/\mu)$; here $\bar{g}$ is the time- and space-average mass-transfer coefficient as defined in equation (2.1.2), Γ is the mass flow rate of liquid per unit width of film, and $a_{g,x}$ is the component of the gravitational acceleration acting in the direction of flow. The parameter in each figure is the length of the measuring electrode, L. We shall forgo comment on the results until later: we first present a method of correlating the data in a compact form which allows us as well to draw some conclusions as to the nature of the flow in the vicinity of the wall.

2.3. *A mass-transfer theory*

We derive here a calculation procedure for heat or mass transfer to film flows which is based on some aspects of boundary-layer theory. We consider an idealised form of film flow in which (a) gradients of concentration exist only in the region near the wall where the shear stress in the liquid does not differ appreciably from the value at the wall,† and (b) the non-dimensional total viscosity $\varepsilon_u^+(\equiv 1 + \mu_t/\mu)$ is a function of only the non-dimensional velocity $u^+(\equiv \bar{u}/(\tau_S/\rho)^{\frac{1}{2}})$. Here μ_t is the eddy viscosity, $\bar{u}$ is the time-averaged velocity in the x direction, τ_S is the shear stress at the wall, and μ is the molecular viscosity of the liquid. The details of the development are given in the Appendix. The theory has two main components:

(1) A method outlined by one of the present authors [1, 4], for the calculation of heat- or mass-transfer rates through uniform-property

† This is a reasonable assumption for large N_{Sc}.

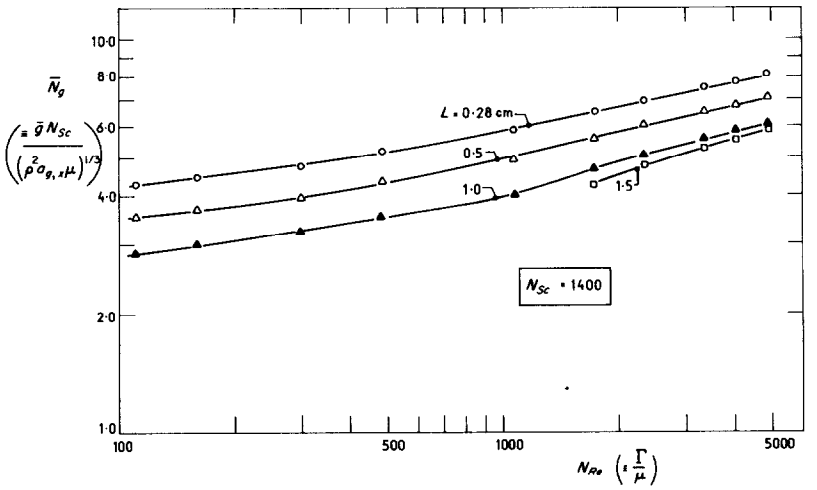

(a)

FIG. 3. Experimental data in the form of a non-dimensional mass-transfer coefficient $\bar{N}_g$ as a function of N_{Re}, for various electrode lengths.

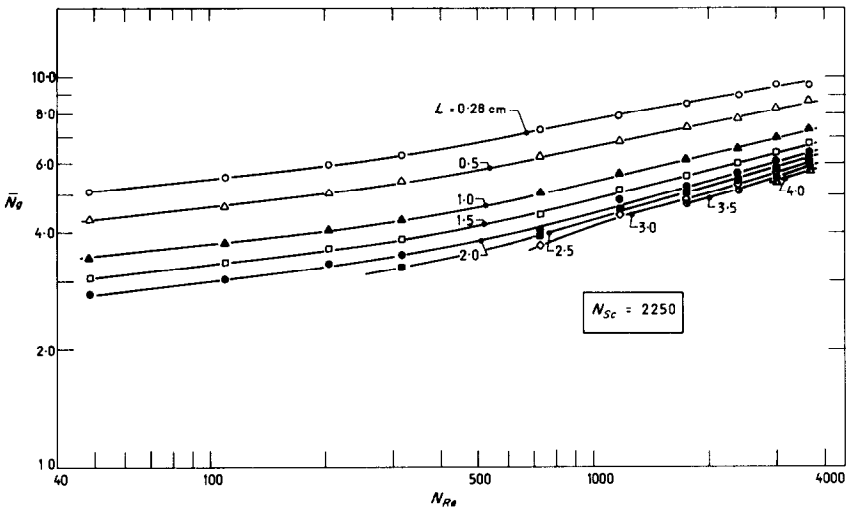

(b)

FIG. 3—*continued.*

boundary layers is adapted (Appendix A.1) to film flows. The modified theory relates the mass-transfer coefficient to a non-dimensional film thickness, the length of the mass-transfer surface, and the transport properties of the liquid.

(2) The non-dimensional film thickness is related, by further application of boundary-layer theory, to the film Reynolds number. The derivation is given in Appendix A.2.

The important results of the theory are summarized below:

(1) The mass-transfer coefficient is related to the independent variables by a function of the form†:

$$\bar{S} = \bar{S}(L^+, N_{Sc}/N_{Sc,t}), \qquad (2.3.1)$$

† The notation $\bar{S}(\ldots, \ldots)$ implies that $\bar{S}$ is a function of the quantities enclosed in the brackets.

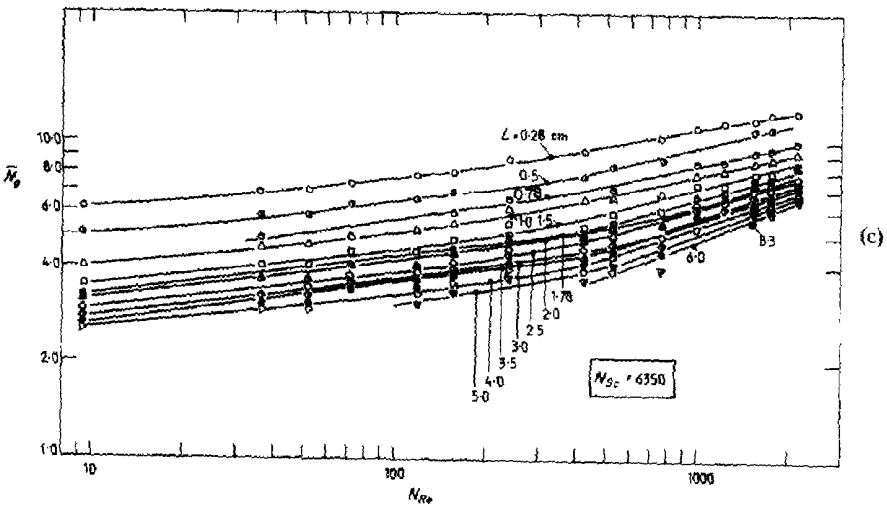

(c)

FIG. 3—*continued.*

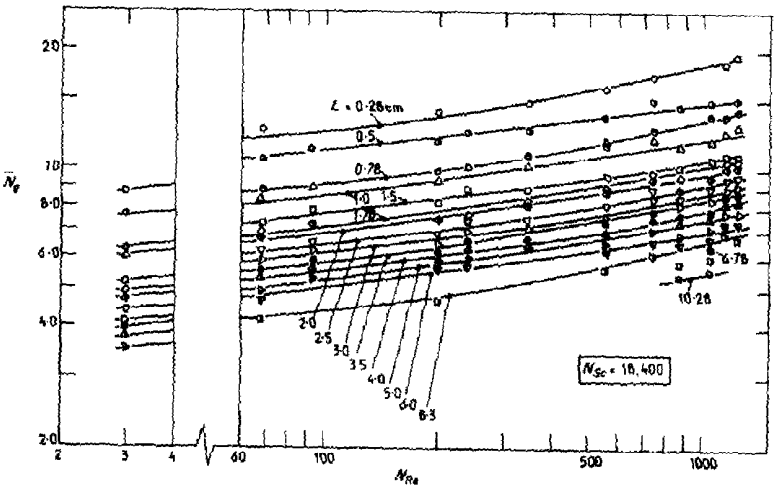

(d)

FIG. 3—*continued.*

where:

(i) $\bar{S} \equiv \dfrac{\bar{g} N_{Sc}}{(\mu \rho^2 a_{g,x})^{\frac{1}{3}} \delta^{+\frac{1}{3}}}$,

and

$$L^+ \equiv \frac{L}{N_{Sc,t}} \left[\frac{a_{g,x} \rho^2}{\mu^2}\right]^{\frac{1}{3}} \delta^{+\frac{1}{3}};$$

(ii) δ^+ stands for the non-dimensional film thickness; this is a function of Reynolds number derived in Appendix A.2 and displayed in Fig. 4.

Here,

$\delta^+ \equiv \delta^{\frac{1}{3}} a_{g,x}^{\frac{1}{2}} \rho/\mu$, a non-dimensional film thickness,

$\delta \equiv$ the average film thickness,

$N_{Sc,t} \equiv$ the turbulent Schmidt number, taken as a constant = 0·9,

$L \equiv$ the length of the mass-transfer surface.

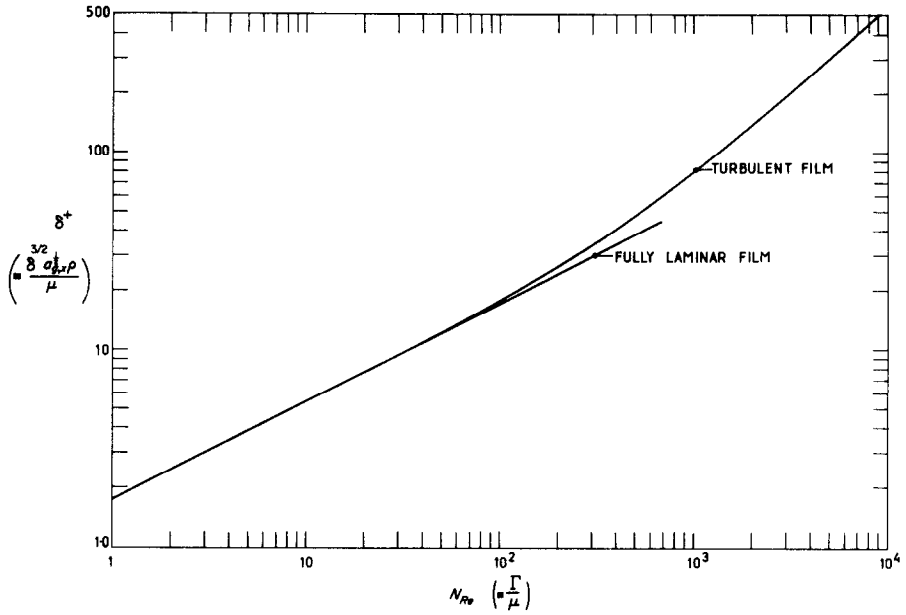

FIG. 4. Non-dimensional mean film thickness, δ^+, as a function of N_{Re}.

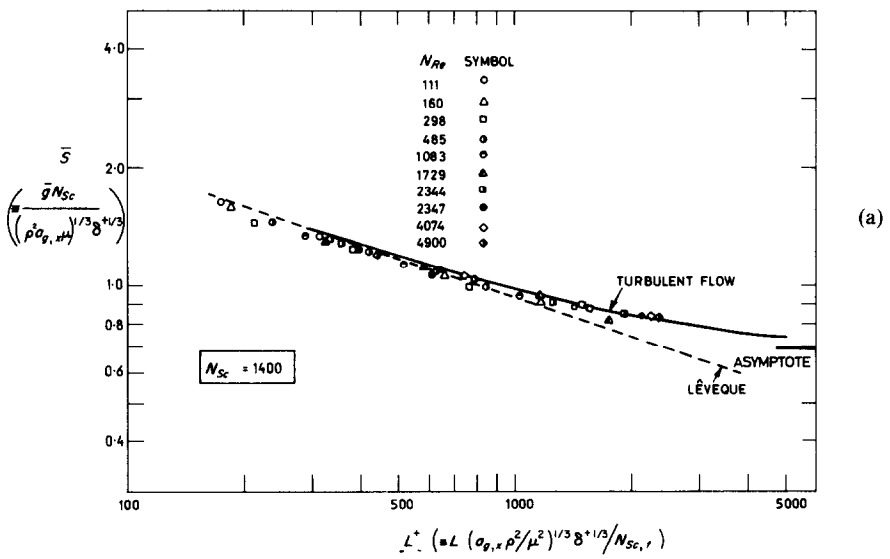

(a)

FIG. 5. Electrolytic mass-transfer data in $\bar{S} \sim L^+$ form.

One of the implications of equation (2.3.1) is that the mass-transfer data for a given liquid (i.e. for fixed $N_{Sc}/N_{Sc,t}$) should fall on a single curve when plotted in the $\bar{S}, L^+$ plane, irrespective of the values of N_{Re} or L.

(2) Particular hypotheses for the distribution of the total viscosity in the film permit us to calculate particular relations between $\bar{S}$, L^+ and $N_{Sc}/N_{Sc,t}$; we have employed here the total-viscosity hypothesis of Van Driest [5]. The

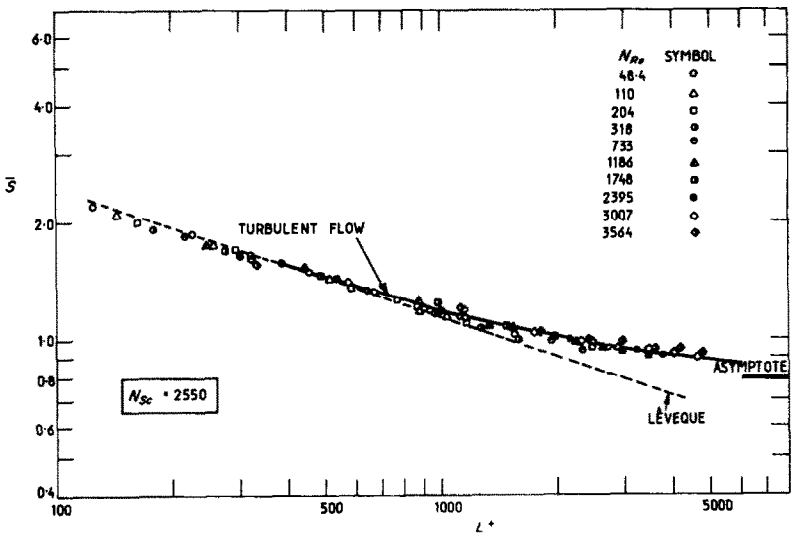

(b)

FIG. 5—*continued.*

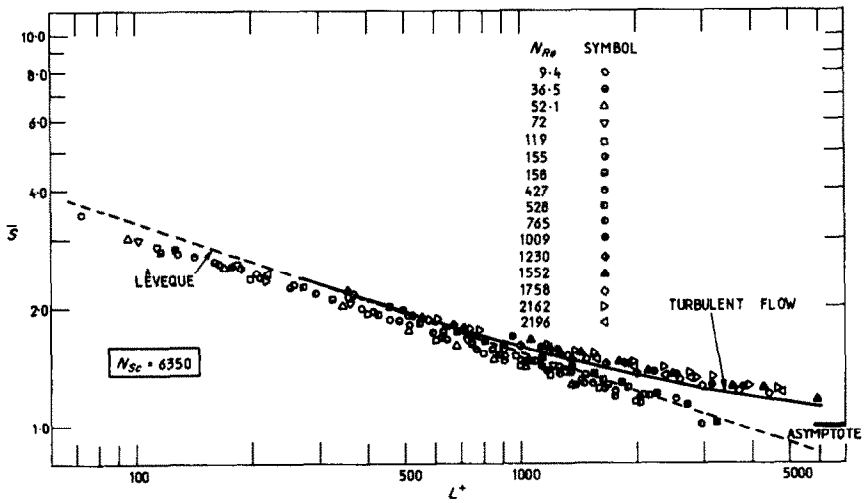

(c)

FIG. 5—*continued.*

theoretically derived $\bar{S} \sim L^+$ relation for the relevant value of $N_{Sc}/N_{Sc,t}$ is shown as a solid curve in each of Figs. 5 (a–d).

(3) The $\bar{S}$ function possesses two asymptotes.

(i) When the concentration gradients are contained within a region of laminar flow, the function is given by† [1]

$$\bar{S} = 0{\cdot}807\,[L^+/(N_{Sc}/N_{Sc,t})]^{-\frac{1}{3}}. \quad (2.3.2)$$

We shall refer to equation (2.3.2) as the Lêveque solution, because it was first derived, albeit in a different form, by Lêveque [7]. It is represented by the broken straight lines in Figs. 5(a–d).

Equation (2.3.2) is valid, according to the theory, whenever the concentration boundary layer is confined to a laminar region. If the film is turbulent, this condition is fulfilled only for L^+ below about 10^3; for a wholly laminar film, or one for which transition is incomplete,

† It can be shown that when the relation $\delta^+ = (3N_{Re})^{\frac{1}{3}}$ appropriate to laminar flow is inserted in (2.3.2), the present theory and that derived by Nusselt [6] (which is restricted to laminar flow) yield identical predictions.

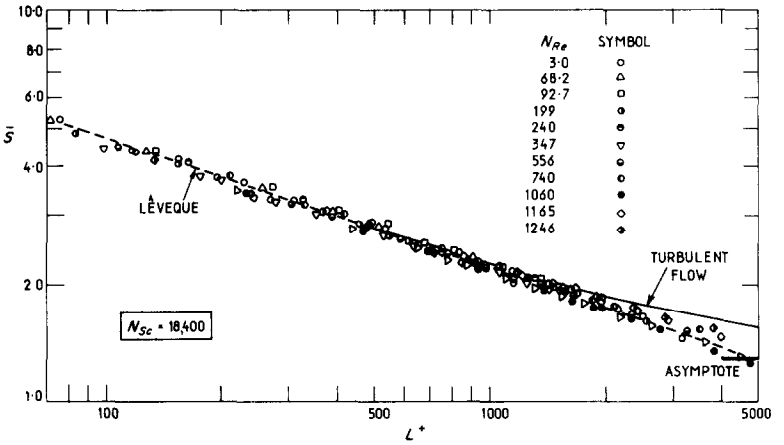

(d)

FIG. 5—*continued.*

equation (2.3.2) may be expected to hold for much larger L^+.

(ii) For turbulent films, large $N_{Sc}/N_{Sc,t}$ and very large L^+, the function takes the form

$$\bar{S} = (N_{Sc}/N_{Sc,t})/P(N_{Sc}/N_{Sc,t}). \quad (2.3.3)$$

The $P(N_{Sc}/N_{Sc,t})$ function is related to, and may be derived from, the total-viscosity profiles. For values of $N_{Sc}/N_{Sc,t}$ greater than 100 the following P-function is obtained from the Van Driest total-viscosity profile:

$$P = 8{\cdot}95\,(N_{Sc}/N_{Sc,t})^{\frac{1}{2}}. \quad (2.3.4)$$

The asymptotic values of $\bar{S}$ computed from equations (2.3.3) and (2.3.4) are shown on the right-hand ordinate axes of the figures.

2.4. *Experimental data in $\bar{S} \sim L^+$ form*

The data shown previously in Figs. 3(a–d) have been recast into $\bar{S} \sim L^+$ form, and are displayed in Figs. 5(a–d). The symbols employed in the figures correspond to different Reynolds numbers; a key to the symbols appears in each figure. The $\delta^+(N_{Re})$ function shown in Fig. 4 was employed in the computation of $\bar{S}$ and L^+.

Other experimental data. Kramers and Kreyger [8] report measurements of the rate of dissolution of a benzoic acid surface into a film of water. Their data are plotted in $\bar{S}$, L^+ coordinates in Fig. 6. The symbols in the figure denote values of N_{Re} and also the various angles of the surface with the horizontal; a key to the symbols is given in the figure.

3. DISCUSSION

3.1. *Comparison of predictions with experimental data for diffusion-controlled electrolysis*

The suitability of the $\bar{S} \sim L^+$ coordinate system. Comparison of Figs. 3(a–d) with Figs. 5(a–d), which display the same experimental data in two different coordinate systems, shows that the second system is much more successful than the former in bringing the data on to a single curve. This fact is in accordance with the hypothesis that the profiles of velocity, total viscosity and total diffusivity indeed possess a universal character.

Strictly speaking, the data tend to lie on one or other of two different curves; Fig. 5(c) illustrates this tendency with particular clarity. The lower of the curves is a straight line of slope $-\frac{1}{3}$; the data for the lower Reynolds numbers lie near this. The upper curve, which is asymptotic on the left to the lower one, is representative mainly of the Reynolds numbers in excess of 1000. This behavior is consistent with the hypothesis that the boundary layer is laminar for Reynolds numbers up to about 700 and turbulent for Reynolds numbers above 1000. The data do not allow the transition range of Reynolds number to be determined to finer limits.

It should be pointed out that the range quoted here may not hold for liquids with viscosity or surface-tension coefficient widely different from the liquids employed in the present tests; for these, the effects of wave formation may be more important than in our investigation.

It can be concluded that the theory for turbulent films is as reliable as that for laminar films in predicting the rate of mass transfer.

It should be mentioned that the data deviate from the plotted theoretical curve considerably less than they do from theoretical curves based

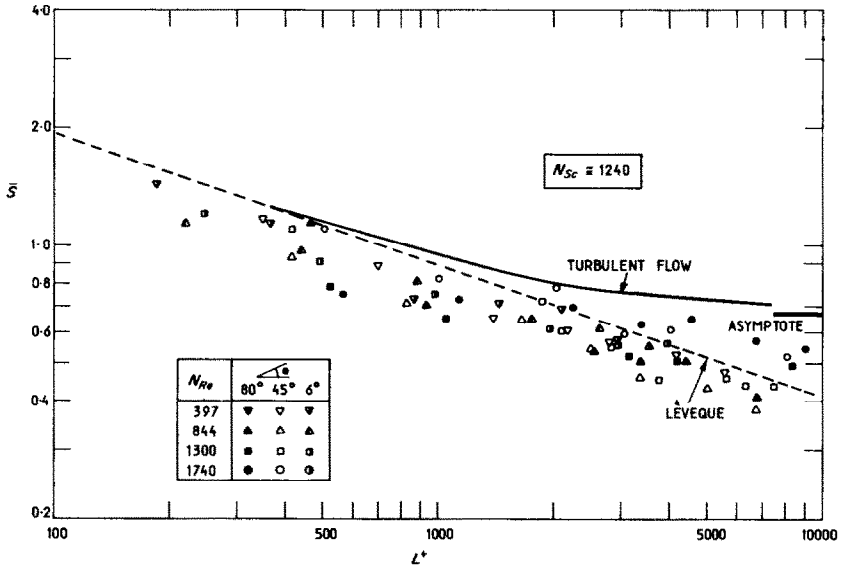

FIG. 6. Dissolution of benzoic acid mass-transfer data in $\bar{S} \sim L^+$ form.

Comparison with predictions for laminar films. Examination of the data for values of L^+ which are less than about 10^3 shows that the experimental mass-transfer rates (proportional to $\bar{S}$) lie close to, or a little below, the values given by the Lêveque solution [equation (2.3.2)]. Discrepancies of up to 10 per cent are found. These deviations may be caused by one or both of the following: (i) incorrectly assumed values of the diffusion coefficients or viscosities of the various mixtures; (ii) spreading of the concentration profile into parts of the film in which the shear stress is significantly smaller than that at the wall.

Comparison with predictions for turbulent flow. The data for the higher Reynolds numbers lie quite near to the curve deduced from the Van Driest total-viscosity hypothesis by the method outlined above and described in the Appendices. on other total-viscosity hypotheses, for example those of Spalding [9] and Rasmussen and Karamcheti [10]. This is further confirmation that the Van Driest equation is among the best that have been proposed so far. It is to be expected that the Deissler [11] equation would be about as good as that of Van Driest, because, though this equation has a different, and for our purposes less convenient, form, numerical values of total viscosities are very nearly the same.

3.2. *Comparison of predictions with experimental data for the dissolution of benzoic acid*

Inspection of Fig. 6 reveals that the experimental data for the dissolution of benzoic acid in water do not collapse on to a single curve, or pair of curves. In view of the more regular behavior of the electrolytic data, the spread

of the benzoic-acid data can be plausibly attributed to experimental scatter.

Perhaps therefore the most important conclusion to draw from Figs. 5 and 6 is that diffusion-controlled electrolysis does afford, when suitable precautions are taken, an unusually accurate means of measurement of mass-transfer phenomena.

3.3. *Practical conclusions*

Figures 5(a–d) strongly suggest that mass-transfer rates between solid surfaces and falling liquid films can be predicted by the following procedure:

(i) Calculate the Reynolds number of the film, and from the curve in Fig. 4, determine the value of δ^+.

(ii) Hence, and from other relevant data, calculate L^+, the non-dimensional length of the mass-transfer surface.

(iii) Then, by reference to graphical representation of the $\bar{S}$ function, $\bar{S}$ is calculated for the relevant L^+ and N_{Sc} values. If N_{Re} is below 700, the laminar-film (Lêveque) version of the $\bar{S}$ function is to be used; above an N_{Re} value of 1000, the turbulent-film value is appropriate; intermediate values must be expected for intermediate Reynolds numbers.

(iv) Finally, the value of the average mass-transfer coefficient $\bar{g}$ is calculated from the definition of $\bar{S}$ and the appropriate fluid properties.

To aid in such calculations, Fig. 7 is presented. This contains, for a wide range of Schmidt numbers, the $\bar{S} \sim L^+$ relation for turbulent films. The left-hand asymptotes of these curves can be used, when produced to the right, for the calculation of laminar films. The curves are based on the Van Driest hypothesis, and on the theory already described. Although the confirmatory experimental data have been confined to the Schmidt-number range from 1400 to 18400, the theoretical foundation appears to be sound enough to permit cautious use of the chart at much lower Schmidt numbers, or of course, if heat transfer is in question, Prandtl numbers.

The particular merit of the above proposal is that the calculation of the mass-transfer rate has been reduced to the successive employment of one universal function with a single argument, namely $\delta^+(N_{Re})$, and a second universal func-

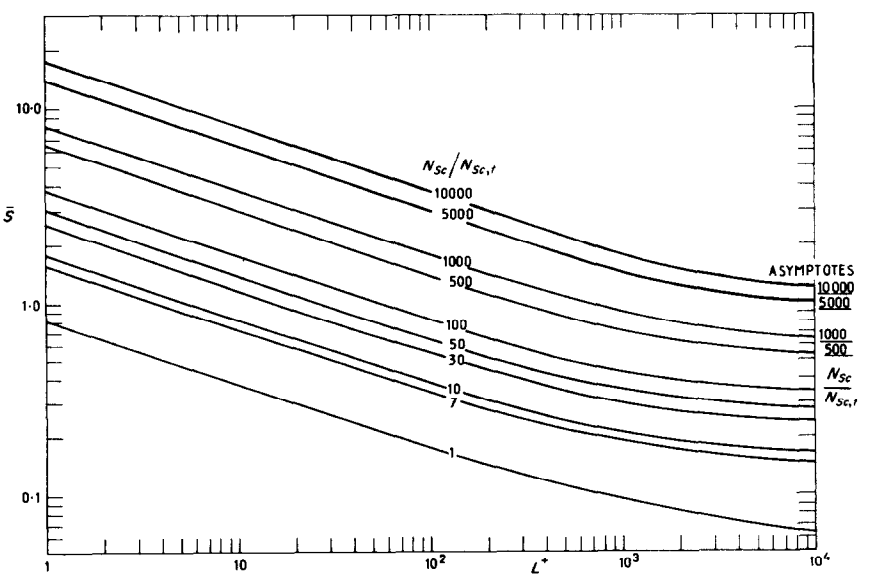

FIG. 7. Theoretically derived $\bar{S} \sim L^+$ relations for various $N_{Sc}/N_{Sc,t}$.

tion having two arguments, namely $\bar{S}(L^+, N_{Sc}/N_{Sc,t})$. If these, or equivalent, functions are not used, it is necessary to employ a three-argument function, for example $\bar{N}_g(N_{Re}, L^3 a_{g,x} \rho^2/\Gamma^2, N_{Sc})$. Three-argument functions are of course always difficult to present graphically.

ACKNOWLEDGEMENTS

One of the authors (A.D.G.) gratefully acknowledges the support of the National Research Council of Canada.

REFERENCES

1. D. B. SPALDING, Contribution to the theory of heat transfer across a turbulent boundary layer, *Int. J. Heat Mass Transfer* **7**, 743–761 (1964).
2. M. EISENBERG, C. W. TOBIAS and C. WILKE, Ionic mass transfer and concentration polarization at rotating electrodes, *J. Electrochem. Soc.* **101**(6), 306 (1954).
3. C. S. LIN, E. B. DENTON, H. S. GASKILL and G. L. PUTNAM, Diffusion-controlled electrode reactions, *Ind. Engng Chem.* **43**(9), 2136–2143 (1951).
4. D. B. SPALDING, Heat transfer to a turbulent stream from a surface with a step-wise discontinuity in wall temperature, in *International Developments in Heat Transfer*, part II, pp. 439–446. *Am. Soc. Mech. Engrs*, New York (1961).
5. E. R. VAN DRIEST, On turbulent flow near a wall, *J. Aeronaut. Sci.* **23**, 1007 (1956).
6. W. NUSSELT, Der Wärmeaustausch am Berieselungskühler, *Z. Ver. Dt. Ing.* **67**, 206–210 (1923).
7. M. A. LÊVEQUE, Les lois de la transmission de la chaleur par convection, *Annls Mines Belg.* **13**, 201, 305, 38 (1928).
8. H. KRAMERS and P. J. KREYGER, Mass transfer between a flat surface and a falling liquid film, *Chem. Engng Sci.* **6**, 42–48 (1956).
9. D. B. SPALDING, A single formula for the law of the wall, *J. Appl. Mech.* **83**, 455–458 (1961).
10. M. RASMUSSEN and K. KARAMCHETI, On the viscous sublayer of an incompressible turbulent boundary layer, SUDAER, Department of Aeronautics and Astronautics, Stanford University (February 1965).
11. R. G. DEISSLER, Analysis of turbulent heat transfer and friction in smooth pipes at high Prandtl or Schmidt numbers, NACA TN 3145 (1954).
12. E. BAKER, Series solution for heat transfer through a turbulent boundary layer, *Int. J. Heat Mass Transfer* **9**, 417–426 (1966).
13. S. V. PATANKAR, Heat transfer across a turbulent boundary layer: application of a profile method to the step-wall temperature problem, *Int. J. Heat Mass Transfer* **9**, 829–834 (1966).
14. G. O. GARDNER and J. KESTIN, Calculation of the Spalding function over a range of Prandtl numbers, *Int. J. Heat Mass Transfer* **6**, 289–299 (1963).
15. C. L. V. JAYATILLAKA, The influence of Prandtl number and surface roughness on the resistance of the laminar sublayer to momentum and heat transfer, Technical note TWF/R/2, Dept. Mech. Engng, Imperial College (January 1966).
16. S. V. PATANKAR, Wall-shear-stress and heat-flux laws for turbulent boundary layer with pressure gradient: use of Van Driest's eddy-viscosity hypothesis, Technical note TWF/TN/14, Dept. Mech. Engng, Imperial College (May 1966).
17. A. E. DUKLER and M. WICKS, Gas–liquid flow in conduits, in *Modern Chemical Engineering*, Vol. 1, pp. 349–435. Reinhold, New York (1963).
18. S. S. KUTATELADZE, *Fundamentals of Heat Transfer*, pp. 308–311. Arnold, London (1963).
19. J. C. BAZAN and A. J. ARVIA, The diffusion of ferro- and ferricyanide ions in aqueous solutions of sodium hydroxide, *Electrochem. Acta* **10**, 1025–1032 (1965).
20. P. L. DUFFIELD, Diffusion-controlled electrolysis at a porous electrode, with gas injection, Ph.D. Thesis, Dept. Mech. Engng, Imperial College (1966).
21. G. D. FULFORD, The flow of liquids in thin films, in *Advances in Chemical Engineering*, Vol. 5, pp. 151–236. Academic Press, New York (1964).

APPENDIX

A.1. *The Mass-transfer Problem*

Spalding [1, 4] has shown that the distribution of the concentration of a diffusing species in a constant-property universal boundary layer is governed by the following partial differential equation (the coordinate system is shown in Fig. 1):

$$\frac{\partial \varphi}{\partial (x^+/N_{Sc,t})} = \frac{1}{u^+ \varepsilon_u^+} \frac{\partial}{\partial u^+} \left(\frac{\varepsilon_\varphi^+}{\varepsilon_u^+} \frac{\partial \varphi}{\partial u^+} \right) \qquad \text{(A.1.1)}$$

where

$\varepsilon_\varphi^+ \equiv \rho(\mathscr{D} + \mathscr{D}_t)/\mu = \rho$ (molecular + eddy diffusivity)/molecular viscosity, non-dimensional total diffusivity,

$\varepsilon_u^+ \equiv (\mu + \mu_t)/\mu =$ (molecular + eddy viscosity)/molecular viscosity, non-dimensional total viscosity,

$x^+ \equiv \int_0^x (\tau_S \rho)^{\frac{1}{2}} \mu^{-1} \, dx$, a non-dimensional length,

$N_{Sc,t} \equiv$ turbulent Schmidt number, taken below as a constant, ($= 0{\cdot}9$).

$u^+ \equiv \bar{u}/(\tau_S/\rho)^{\frac{1}{2}}$, non-dimensional velocity,

$\varphi \equiv$ concentration of diffusing species, g/g solution,

$\bar{u} \equiv$ time-averaged velocity in the x direction,

$\rho \equiv$ density of the liquid,

$\tau_S \equiv$ shear stress at the wall.

It is a common assumption that the following relation holds between ε_φ^+ and ε_u^+;

$$\varepsilon_\varphi^+ = \frac{N_{Sc,t}}{N_{Sc}} + \varepsilon_u^+ - 1 \qquad \text{(A.1.2)}$$

further, ε_u^+ is held to depend upon u^+ alone. Equation (A.1.1) can be integrated† for a given set of boundary conditions and a particular $\varepsilon_u^+(u^+)$ function to yield the concentration distribution in the boundary layer; the local mass-transfer coefficient can then be evaluated from the gradient of the concentration at the wall.

The mathematical form of the solution for the present boundary conditions. It can be shown (see, for example, [1]) that for the condition of a step change in the concentration at the wall, the solution of equation A.1.1 leads to a relation of the form:

$$S \equiv gN_{Sc}/(\tau_S\rho)^{\frac{1}{2}} = S(x^+/N_{Sc,t}, N_{Sc}/N_{Sc,t}) \qquad \text{(A.1.3)}$$

where $g \equiv \dot{m}''/(\varphi_G - \varphi_S)$, and $\dot{m}''$ is the local mass flux at the surface. For purposes of comparison of the predictions of the theory with existing experimental data, we require the equivalent relationship for the *average* mass-transfer coefficient; the relationship is obtained as follows:

$$\bar{S} \equiv \frac{\bar{g}N_{Sc}}{(\tau_S\rho)^{\frac{1}{2}}} = \int_0^{L^+} \frac{S}{L^+}\,\mathrm{d}(x^+/N_{Sc,t}) = \bar{S}(L^+, N_{Sc}/N_{Sc,t}) \qquad \text{(A.1.4)}$$

where

$L^+ \equiv \int_0^L (\tau_S\rho)^{\frac{1}{2}}(\mu N_{Sc,t})^{-1}\,\mathrm{d}x$,

$\bar{g} \equiv \bar{\dot{m}}''/(\varphi_G - \varphi_S)$, as defined in equation (2.1.2),

$L \equiv$ length of the mass-transfer surface.

The $\bar{S}(L^+, N_{Sc}/N_{Sc,t})$ function. Equation (A.1.1) possesses two asymptotic solutions. The first, which is of interest in the present work, is obtained for conditions of laminar flow, or turbulent flow and small L^+; under these conditions ε_u^+ can be placed equal to unity in equations (A.1.1) and (A.1.2). The problem then reduces to one which was first solved by Lèveque [7]. Its solution is

$$\bar{S} = 0{\cdot}807\,[L^+(/N_{Sc}/N_{Sc,t})]^{-\frac{1}{3}}. \qquad \text{(A.1.5)}$$

The second asymptotic solution, which is valid for turbulent flow, large $N_{Sc}/N_{Sc,t}$ and very large L^+, is obtained by setting the left-hand side of (A.1.1) equal to zero; physically this corresponds to conditions when the mass-transfer coefficient is independent of L. The solution is

$$\bar{S} = (N_{Sc}/N_{Sc,t})/P(N_{Sc}/N_{Sc,t}) \qquad \text{(A.1.6)}$$

It is shown in [1] that the P-function is related to, and may be derived from, the total-viscosity profile.

Solutions of the partial differential equation which hold for turbulent flows and intermediate values of L^+ have been obtained here by an approximate method developed by Patankar [13], and shown by him to give an error of less than 2 per cent in our conditions. The following total-viscosity formula proposed by Van Driest [5] was employed†

$$\varepsilon_u^+ = \{1 + \sqrt{(1 + 4\varkappa^2 y^{+2}[1 - \exp(-y^+/A_*)]^2)}\}/2 \qquad \text{(A.1.7)}$$

where

$y^+ \equiv y(\tau_S\rho)^{\frac{1}{2}}/\mu$,

$y \equiv$ distance normal to wall,

$A_*, \varkappa \equiv$ constants.

The values of the constants used were $\varkappa = 0{\cdot}4$ and $A_* = 26$. The associated P-function is given by

$$P = 8{\cdot}95\,(N_{Sc}/N_{Sc,t})^{\frac{1}{2}} \qquad \text{(A.1.8)}$$

for values of N_{Sc} greater than approximately 100.

Examples of the theoretically derived

† Approximate methods of solution are given by Baker [12] and Patankar [13]. Some exact numerical solutions for boundary conditions equivalent to those considered here have been published by Gardner and Kestin [14].

† The Van Driest hypothesis has been employed on the basis of the recommendations of Jayatillaka [15] and Patankar [16].

$\bar{S}(L^+, N_{Sc}/N_{Sc,t})$ functions are shown in Figs. 5(a–d), 6 and 7. In each figure, equation (A.1.5) is represented by a broken straight line, and the numerically computed solutions are shown as solid curves. The asymptotic values of $\bar{S}$ for large L^+ are given on the right-hand ordinate axes of the figures.

Adaptation to film flows. We intend to relate the wall shear stress, τ_S, which appears in the groups $\bar{S}$ and L^+, to the relevant independent variables for falling liquid films. At present we are concerned with circumstances in which the only important external forces which act on the film are the wall shear and the force of gravity. If these forces are in equilibrium we can derive, by way of a force balance, the relation $\tau_S = \rho\delta a_{g,x}$ where δ is the film thickness. It is convenient at this stage to introduce a non-dimensional film thickness which is defined as

$$\delta^+ \equiv \delta(\tau_S\rho)^{\frac{1}{2}}/\mu = \delta^{\frac{1}{2}} a_{g,x}^{\frac{1}{2}}\,\rho/\mu. \qquad \text{(A.1.9)}$$

If we now substitute for τ_S in terms of δ^+ in the groups $\bar{S}$ and L^+, we obtain

$$\bar{S} = \frac{gN_{Sc}}{(\mu\rho^2 a_{g,x})^{\frac{1}{3}}\,\delta^{+\frac{1}{3}}}$$

and

$$L^+ = \frac{L}{N_{Sc,t}}\left(\frac{a_{g,x}\rho^2}{\mu^2}\right)^{\frac{1}{3}}\delta^{+\frac{1}{3}}. \qquad \text{(A.1.10)}$$

In the final stage of the analysis, which is given below, we derive a relationship between δ^+ and the film Reynolds number.

A.2. *The $\delta^+ \sim N_{Re}$ Function*

Theoretical studies of the hydrodynamics of film flows have been carried out by Dukler [17] and Kutateladze [18], among others. In order to provide a complete picture of the application of boundary-layer theory to film flows, we give below a brief derivation of a hydrodynamic theory which is similar in most respects to those of Dukler and Kutateladze; the main difference is that we employ a single formula for the distribution of the total viscosity in the film.

The equations of motion and continuity for the film are as follows:

(i) Equation of motion;

$$\frac{\tau}{\tau_S} \equiv \varepsilon_u^+ \frac{du^+}{dy^+} = 1 - \frac{y^+}{\delta^+}. \qquad \text{(A.2.1)}$$

where

$\tau \equiv$ shear stress in the film in a plane parallel to the surface, at a distance y from the wall,

$y^+ \equiv y(\tau_S\rho)^{\frac{1}{2}}/\mu.$

(ii) Continuity;

$$N_{Re} \equiv \frac{\Gamma}{\mu} = \int_0^{\delta^+} u^+\,dy^+. \qquad \text{(A.2.2)}$$

For the present work we have employed the following ε_u^+ expression derived from the Spalding [9] velocity profile;

$$\varepsilon_u^+ = 1 + \kappa/E\,[\exp \kappa u^+ - 1 - \kappa u^+ - (\kappa u^+)^2/2! - (\kappa u^+)^3/3!] \qquad \text{(A.2.3)}$$

where $\kappa = 0{\cdot}4$ and $E = 12$.

The solution of the equations is straightforward; substitution of (A.2.3) into (A.2.1) and integration† yields the velocity distribution in the film, $u^+(y^+, \delta^+)$. The $\delta^+(N_{Re})$ function can then be obtained by substitution of the velocity profile expression into (A.2.2) and integration of the quadrature (in the present case it was necessary to employ a numerical method). The result is given in Fig. 4.

In practice it has been found [21] that wave formation occurs at the free surface of the film over the greater part of the span of N_{Re} of practical interest. However Fulford [21] and Dukler [17] have shown that if δ is defined as the *mean* film thickness there is reasonable agree-

† The choice of the total-viscosity profile (A.2.3) was made for the following reasons: (a) an analytical expression is obtained for the velocity distribution, whereas use of the Van Driest formula would necessitate numerical integration, and (b) there is no significant difference between the $\delta^+(N_{Re})$ functions derived from either profile.

ment between theoretical $\delta^+(N_{Re})$ functions virtually identical to the one derived here and experimental data. It should be pointed out that the scatter in the film thickness data is large (of the order of 20 per cent). Note that in the present work the effects of errors in the estimation of δ^+ are diminished by the fact that this quantity appears to the one-third power in $\bar{S}$ and L^+.

Résumé—Le coefficient de transport de masse entre un film liquide s'écoulant sur une surface verticale a été mesuré à l'aide de la technique du transport de masse électrolytique contrôlé par la diffusion. Les mesures sont comparées avec les prévisions basées sur une adaptation aux écoulements de film d'une théorie de l'un des auteurs pour le transport de chaleur ou de masse à travers les couches limites. Il y a un bon accord entre la théorie et l'expérience pourvu que le nombre de Reynolds du film soit en dehors de la gamme d'environ 700 à 1000.

Zusammenfassung—Für den Massenübergangskoeffizienten zwischen einem fallenden Flüssigkeitsfilm und einer senkrechten Oberfläche wurden Messungen durchgeführt; es wurde das Verfahren des diffusionskontrollierten elektrolytischen Massenübergangs angewendet. Die Ergebnisse werden verglichen mit Berechnungen, die auf einer Angleichung an Filmströmungen beruhen entsprechend einer Theorie für Wärme- oder Stofftransport durch Grenzschichten von einem Autor der vorliegenden Arbeit. Es ergibt sich gute Übereinstimmung zwischen Theorie und Versuche unter der Voraussetzung, dass die Reynolds-Zahl, bezogen auf den Film, nicht im Bereich 700 bis 1000 liegt.

Аннотация—Получены результаты для коэффициента массообмена между падающей жидкой пленкой и вертикальной поверхностью; для этой цели использовался метод диффузионно-контролируемого электролитического массообмена. Результаты сравнивались с теоретическими данными, полученными на основе предложенной одним из авторов данной статьи теории тепло-и массообмена в пограничных слоях для случая пленочных течений. Сравнение теоретических и экспериментальных данных дает хорошее соответствие при условии, что число Рейнольдса для пленки не лежит в пределах значений ~700–1000.